Available online at www.sciencedirect.com
SCIENCE DIRECT®
Journal of Solid State Chemistry 178 (2005) 1367–1375
JOURNAL OF SOLID STATE CHEMISTRY
www.elsevier.com/locate/jssc

Redox processes in highly yttrium-doped barium titanate

Anatolii Belous[a], Oleg V'yunov[a,*], Leonid Kovalenko[a], Darko Makovec[b]

[a]*Department of Solid State Chemistry, V.I. Vernadskii Institute of General & Inorganic Chemistry, The Ukrainian National Academy of Sciences, Institute of General & Inorganic Chemistry, 32/42, Palladin Ave, 03680 Kyiv 142, Ukraine*
[b]*Jožef Stefan Institute, Ljubljana, Slovenia*

Received 8 November 2004; received in revised form 17 January 2005; accepted 20 January 2005
Available online 17 March 2005

Abstract

The changes of microstructure occurring during oxidation of the reduced form of yttrium-doped barium titanate ($Ba_{1-x}Y_x^{\bullet}Ti_{1-x}^{4+}Ti_x^{3+}O_3$) have been studied. Samples were sintered under reduction conditions at $P_{O_2} = 10^{-4}$ Pa and oxidized by annealing at high temperatures (1150 and 1350 °C) in air. Depending on yttrium concentration, the oxidation of the reduced form of the yttrium-doped $BaTiO_3$ caused precipitation of the phase $Ba_6Ti_{17}O_{40}$ or the phases $Ba_6Ti_{17}O_{40}$ and $Y_2Ti_2O_7$. The precipitates had well-defined orientational relationships with the perovskite matrix. Oxidation of the reduced form of doped barium titanate results in formation of the phase $Ba_{1-x}Y_x^{\bullet}Ti_{1-x/4}^{4+}(V_{Ti}'''')_{x/4}O_3$ responsible for increase in the resistance of outer grain layers, which lie between grain boundaries and grain.

Keywords: Barium titanate; Yttrium doping; Oxidation; Microstructure; Precipitation; Orientational relationships; Resistance

1. Introduction

Donor-doped polycrystalline barium titanate sintered in air becomes semiconducting and exhibits a property that is important in application—positive temperature coefficient of resistance. The semiconducting properties arise in barium titanate on partial substitution of barium by three-valent ions (for example, Y, La, Nd…) [1,2] or titanium by ions of the fifth or sixth group (for example, Nb, Ta, Mo…) [3,4]. The semiconducting reduced form of barium titanate doped by rare-earth ions, for example, yttrium ions, may be represented by the chemical formula $Ba_{1-x}Y_x^{\bullet}Ti_{1-x}^{4+}Ti_x^{3+}O_3$ [5] (Hereinafter the notation proposed by the author of [6] is used; in particular, $Y^{\bullet}$ denotes the excess positive charge (+1) of yttrium in barium site, andV_{Ti}'''' denotes the negative charge (−4) of titanium vacancies). When barium titanate synthesized in air with small titanium excess, at least majority of Y will incorporate at Ba sites [7]. During cooling after sintering, the ceramic is oxidized, and the dielectric oxidized form of barium titanate is formed, where cation vacancies arise for compensation of the excess charge of donor dopant [8]. In Ref. [9] on the basis of atomistic simulation study of doping processes it was shown that the formation energy of $Y_{Ba}^{\bullet} + V_{Ti}''''$ defect (4.35 eV) is lower than that of $Y_{Ba}^{\bullet} + V_{Ba}''$ defect (7.23 eV). Therefore, the oxidized form of yttrium-doped barium titanate may be represented as $Ba_{1-x}Y_x^{\bullet}Ti_{1-x/4}^{4+}(V_{Ti}'''')_{x/4}O_3$.

An important process in the formation of PTCR properties during sintering in air is the oxidation of grain boundaries on cooling. It is difficult to investigate these oxidation processes using diffraction methods because the doping level does not exceed one percent, and only outer layers of grains are usually oxidized. In order to investigate the processes occurring at grain boundaries, the oxidation processes in the reduced form of fine-grained powders can be investigated supposing that the same processes occur at grain boundaries. In fine-grained powders, the oxidized area increases

*Corresponding author. Fax: +38044 4242211.
E-mail address: vyunov@ionc.kar.net (O. V'yunov).

0022-4596/$ - see front matter © 2005 Published by Elsevier Inc.
doi:10.1016/j.jssc.2005.01.014

substantially, resulting in an increase in the percentage of the phases, which are formed on oxidation and, therefore, it is possible to use diffraction methods for the investigation of phase composition. It is known that, in comparison to the synthesis in air, the degree of substitution of rare-earth elements for barium ions is higher when barium titanate is synthesized in a reducing atmosphere. Therefore, investigating the reduced form of barium titanate after oxidation it is possible to obtain information about the phases, which are formed at grain boundaries at low rare-earth concentration (at which the samples synthesized in air have PTCR effect) and high rare-earth concentration (at which the samples synthesized in air are dielectric, and PTCR effect does not arise). This approach was used by the authors of [8] for investigations of microstructural changes during oxidation of the reduced form of lanthanum-doped barium titanate. Although yttrium-doped barium titanate has good electrophysical characteristics, the redox processes during its synthesis are not described in the literature.

Therefore, the aim of the present work was to study the changes of microstructure during oxidation of the reduced form of yttrium-doped barium titanate ($Ba_{1-x}Y_x^{\bullet}Ti_{1-x}^{4+}Ti_x^{3+}O_3$) and to carry out impedance investigations, which will allow the processes at grain boundaries of PTCR ceramics based on barium titanate, to be understood.

2. Experimental section

Ceramic samples of the reduced form of yttrium-doped barium titanate ($Ba_{1-x}Y_x^{\bullet}Ti_{1-x}^{4+}Ti_x^{3+}O_3$) were prepared by solid-state reaction technique. Extra-pure $BaCO_3$, TiO_2 and Y_2O_3 were used as initial reagents. The powders were mixed in necessary ratio and ball-milled in agate mortar. The mixtures were granulated with addition of 10% polyvinyl alcohol, pressed into pellets (10 mm in diameter and 2 mm thick) by uniaxial pressing at 150 MPa, and sintered under reduction conditions $P_{O_2} = 10^{-4}$ Pa at 1400 °C. Under these conditions, yttrium is incorporated into barium titanate lattice in amounts sufficient for X-ray analysis (yttrium solubility limit under these conditions reaches ca. 4 mol% Y_{Ba} [10], while in the case of sintering in air it does not exceed 1.5 mol% Y_{Ba} [11]). The samples with an yttrium contents of 1 mol% (less than solubility limit in the case of synthesis in air) and 2.5 mol% (more than solubility limit in the case of synthesis in air, but less than solubility limit at $P_{O_2} = 10^{-4}$ Pa) were chosen for investigation. The ratios of cation contents measured using wavelength-dispersive spectroscopy (WDS) in the grains of solid solutions were in good agreement with the nominal compositions of the samples. As-fired ceramic pellets and powder after grinding and milling of ceramics pellet and sifting through a nylon mesh with grid 40×40 μm were used for oxidation. Samples were oxidized at 1150 and 1350 °C during 20 and 1 h, respectively. The powders were used for X-ray investigations, and the tablets were used for electron microscopy.

The phases precipitated during the oxidation process were characterized by X-ray powder diffractometry (XRPD) using DRON-4-07 (Cu$K\alpha$ radiation; 40 kV, 20 MA, step-scan mode with a step size 0.02° and a counting time per data point of 10 s) and transmission electron microscopy (TEM) using JEM 2000 FX, JEOL, Tokyo, Japan (LaB_6 cathode, accelerating voltage 200 kV). Bright-field (BF) and dark-field (DF) imaging in combination with selected area electron diffraction (SAED), microdiffraction (MD), and electron-dispersive X-ray spectroscopy (EDXS) was used.

Dielectric characteristics in microwave range (1 GHz) of samples 1 mm in diameter and 1 mm in height were measured using a coaxial line. Dielectric permittivity was calculated by the technique reported in Ref. [12]. The measurement accuracy of dielectric permittivity (ε) was 12%. Impedance data were obtained using a Solartron PGSTAT-30 impedance analyzer in the range 100 Hz to 1 MHz and a VM-560 Q-meter in the range 50 kHz to 35 MHz.The components of the equivalent circuit were identified using the Frequency Response Analyzer 4.7 program.

3. Results and discussion

Fig. 1 shows diffractograms of a sample of the reduced form of yttrium-doped barium titanate with the nominal formulas $Ba_{0.975}Y_{0.025}Ti_{0.975}^{4+}Ti_{0.025}^{3+}O_3$ before and after oxidation for 20 h at 1150°C in air. The diffractograms shows that the samples of perovskite phase before and after oxidation are tetragonal (space group $P4mm$ [13]).

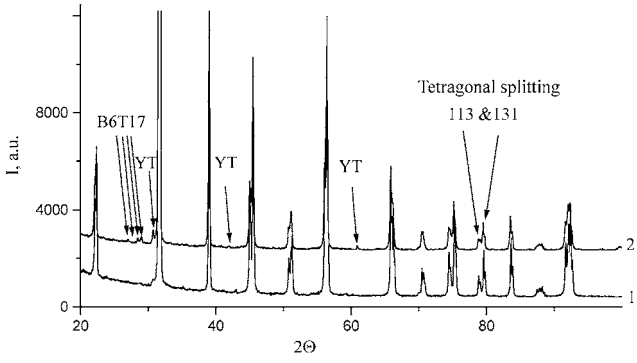

Fig. 1. Diffractograms of yttrium-doped barium titanate with the nominal compositions $Ba_{0.975}Y_{0.025}Ti_{0.975}^{4+}Ti_{0.025}^{3+}O_3$ after sintering in reducing atmosphere, $P_{O_2} = 10^{-4}$ Pa (1) and after oxidation in air for 20 h at 1150 °C (2): $B_6T_{17} = Ba_6Ti_{17}O_{40}$, $YT = Y_2Ti_2O_7$.

At oxidation of ceramic samples for 20 h at 1150 °C, only areas near the surfaces of the pellets were light, which indicated oxidation, which is accompanied by transition $Ti^{3+} \rightarrow Ti^{4+}$, while the inner areas of the pellet remained in dark reduced form. XRPD showed that the material inside the pellet was single-phase, whereas the material near the surface of the pellet was multiphase (see Fig. 1, patterns 2). In addition to the perovskite phase, the cubic compound $Y_2Ti_2O_7$ with pyrochlore structure (space group $Fd\bar{3}m$ (227) [14]) and monoclinic compound $Ba_6Ti_{17}O_{40}$ (space group $C2/c$ (15) [15]) precipitated.

To elucidate the effect of the yttrium content of the $(Ba_{1-x}Y_x)TiO_3$ system on the temperature of phase transition from spontaneously polarized to unpolarized state, electrophysical investigations of undoped barium titanate ($BaTiO_3$), and also yttrium-doped samples $Ba_{0.99}Y_{0.01}Ti^{4+}_{0.99}Ti^{3+}_{0.01}O_3$ and $Ba_{0.975}Y_{0.025}Ti^{4+}_{0.975}Ti^{3+}_{0.025}O_3$ after sintering in reducing atmosphere and after oxidation in air were carried out in the microwave range (1 GHz), where the conductivity does not affect significantly the properties. Results of measurement are shown in Fig. 2. $BaTiO_3$ sample oxidized in air was light throughout its volume, and the maximum of permittivity ε was observed at 120 °C (Fig. 2a). After thermal treatment in reducing atmosphere the maximum shifted in the direction of low temperatures and was diffuse, which may be due to distortion of crystal lattice by the formation of anion vacancies and to partial reduction of titanium ($Ti^{4+} \rightarrow Ti^{3+}$), respectively [16]. Processes of formation of anion vacancies and partial reduction of the titanium in undoped barium titanate are interdependent.

In comparison with undoped barium titanate, in yttrium-doped barium titanate oxidized in air a smearing of $\varepsilon(T)$ peak is observed, which increases with yttrium concentration (Fig. 2). This behaviour is typical of ferroelectric phase with nonferroelectric dopants [17]. After thermal treatment in reducing atmosphere, the smearing of $\varepsilon(T)$ peak is stronger than that observed after firing in air, but the temperature of $\varepsilon(T)$ maximum does not change. This allows one to conclude that the smearing of $\varepsilon(T)$ peak occurs due to partial reduction of titanium, which is associated with incorporation of yttrium ions in barium sublattice and with subsequent decrease in charge in titanium sublattice. After thermal treatment of yttrium-doped barium titanate in reducing atmosphere, anion vacancies are not formed or formed in much smaller numbers in comparison with undoped barium titanate [18], therefore the $\varepsilon(T)$ maximum does not shift.

Figs. 3–5 show micrographs of phases which precipitate on grains of ceramic with nominal composition $Ba_{0.975}Y_{0.025}Ti^{4+}_{0.975}Ti^{3+}_{0.025}O_3$ after oxidation. Investigations of the microstructure of the ceramic show that in the sample with low yttrium concentration

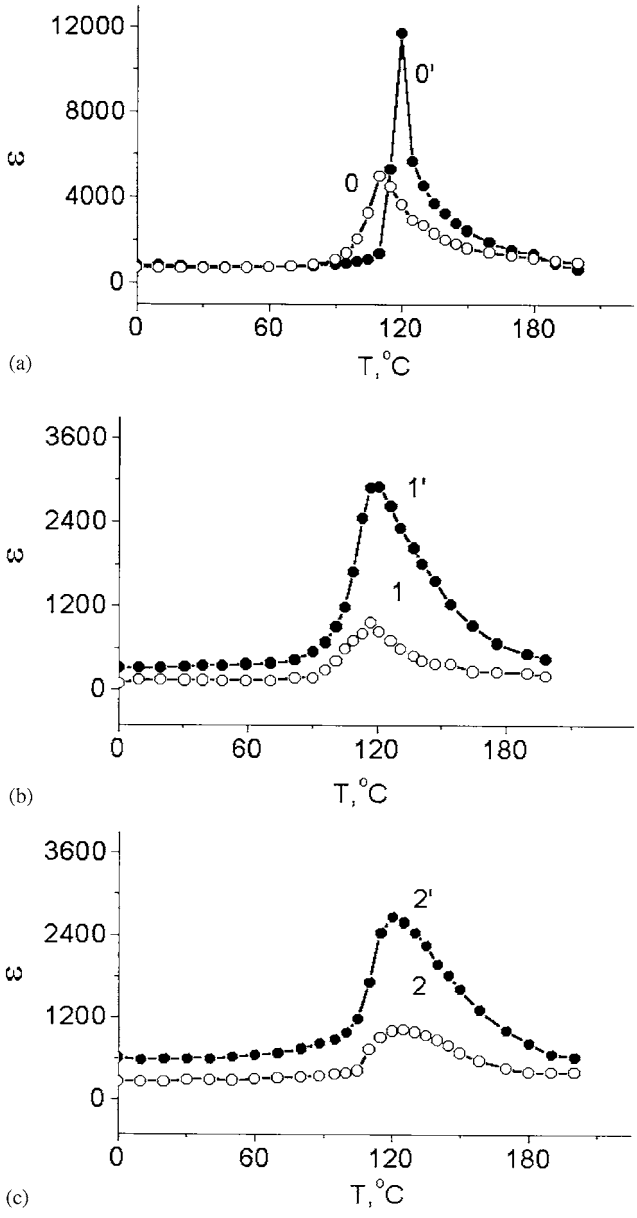

Fig. 2. Temperature dependence of the permittivity of ceramics based on barium titanate, $BaTiO_3$(a), $Ba_{0.99}Y_{0.01}Ti^{4+}_{0.99}Ti^{3+}_{0.01}O_3$ (b) and $Ba_{0.975}Y_{0.025}Ti^{4+}_{0.975}Ti^{3+}_{0.025}O_3$ (c) after sintering in reducing atmosphere, $P_{O_2} = 10^{-4}$ Pa (0, 1, 2), and after oxidation in air for 20 h at 1150 °C (0′, 1′, 2′); test frequency is 1 GHz.

($Ba_{0.99}Y_{0.01}Ti^{4+}_{0.99}Ti^{3+}_{0.01}O_3$), as well as in the sample with the high yttrium concentration ($Ba_{0.975}Y_{0.025}Ti^{4+}_{0.975}Ti^{3+}_{0.025}O_3$) the $Ba_6Ti_{17}O_{40}$ phase precipitates after oxidation, which agrees with the XRPD results. Phase $Ba_6Ti_{17}O_{40}$ was located preferentially inside the matrix grains. It was found in two different forms. Fig. 3 shows TEM image of small bulk precipitates in an oxidized sample with nominal composition $Ba_{0.975}Y_{0.025}Ti^{4+}_{0.975}Ti^{3+}_{0.025}O_3$. The precipitates are concentrated in cluster, nearly rectangular in shape, which lies parallel to the {111} planes of the perovskite structure. From the

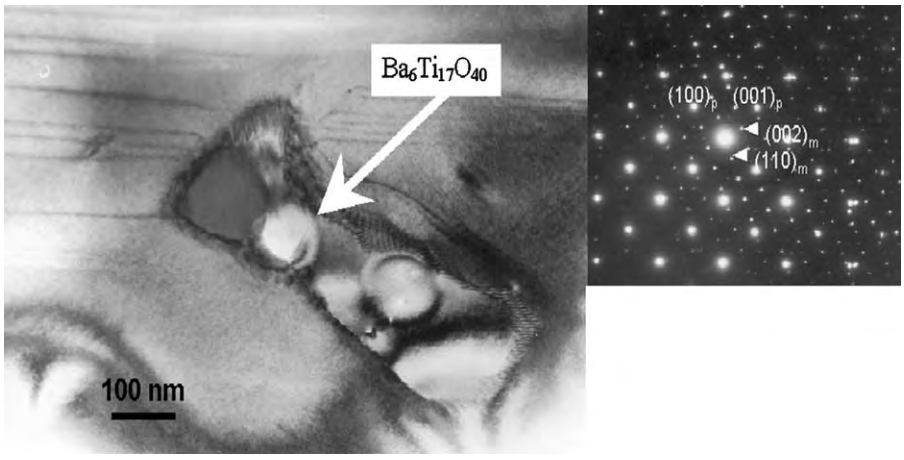

Fig. 3. (a) Micrograph of $Ba_6Ti_{17}O_{40}$phase in matrix grain of sample with nominal composition $Ba_{0.975}Y_{0.025}Ti^{4+}_{0.975}Ti^{3+}_{0.025}O_3$, which precipitates after oxidation in air for 20 h at 1150 °C. (b) Electron diffraction pattern taken in the region of the grain with the precipitate.

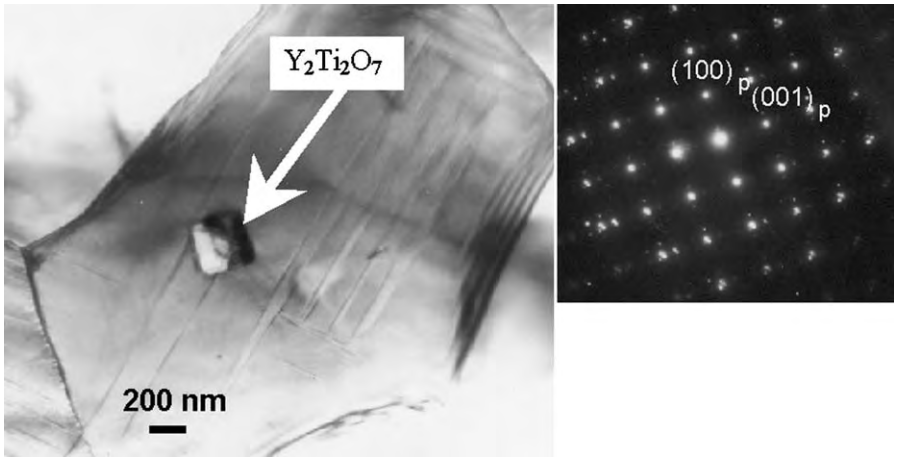

Fig. 4. (a) Micrograph of rectangular $Y_2Ti_2O_7$phase in matrix grain of sample with nominal composition $Ba_{0.975}Y_{0.025}Ti^{4+}_{0.975}Ti^{3+}_{0.025}O_3$, which precipitates after oxidation in air for 20 h at 1150 °C. (b) Electron diffraction pattern taken in the region of the grain with the precipitate, marked by an arrow in (a).

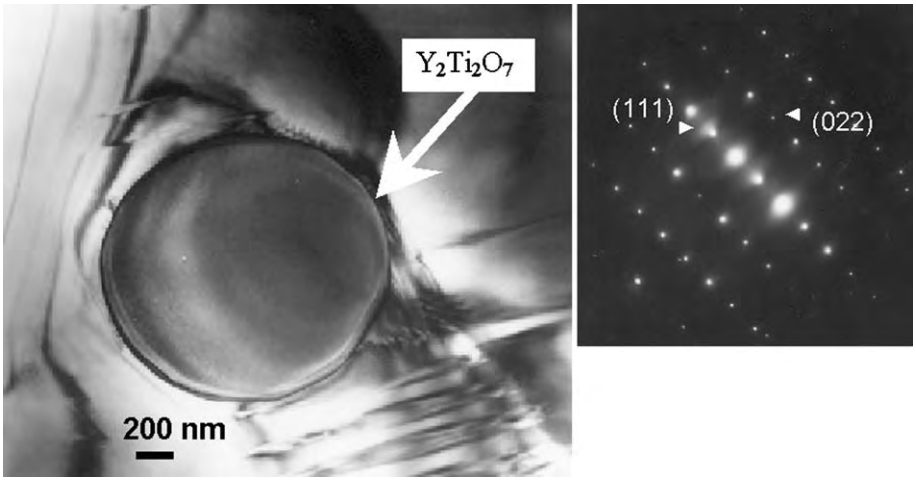

Fig. 5. (a) Micrograph of spherical $Y_2Ti_2O_7$phase in matrix grain of sample with nominal composition $Ba_{0.975}Y_{0.025}Ti^{4+}_{0.975}Ti^{3+}_{0.025}O_3$, which precipitates after oxidation in air for 20 h at 1150 °C. (b) Electron diffraction pattern taken at the precipitate.

electron diffraction pattern taken from the region of the grain with the precipitate, the orientational relationship between the monoclinic compound $Ba_6Ti_{17}O_{40}$ (marked with "m" in Fig. 3b) and the cubic perovskite matrix (marked with "p" in Fig. 3b) was found to be the same as already reported in Refs. [8,19].

Investigations showed that the compound $Ba_6Ti_{17}O_{40}$ also precipitated in the form of thin platelike particles, lying in the perovskite close-packed {111} planes. Such platelike precipitates of the compound $Ba_6Ti_{17}O_{40}$ were also observed during the oxidation of the reduced form of barium titanate doped by lanthanum [8] and cerium [20].

As was shown in Ref. [20], the shape of the precipitates most probably depends on the mode of nucleation. If the precipitate homogeneously nucleates in the {111} planes of the perovskite matrix, it starts as a Ti-rich nonconservative planar fault. Nucleation in this case occurs in the perovskite {111} planes since here a low-energy surface between the two phases is formed. With increasing time or temperature of oxidation the precipitate grows to a certain degree, but remains in the form of a plate. However, if $Ba_6Ti_{17}O_{40}$ heterogeneously nucleates at crystal imperfections inside the matrix grain, for example at dislocations, it will have a bulk form. In the general case, heterogeneous nucleation is energetically more favorable than homogeneous nucleation. In the case of heterogeneous nucleation, the precipitate's form is a compromise between the influence of the interfacial energy and the strain energy, which depends on the precipitate's shape. A precipitate tends to have a minimal interfacial energy and to grow in the directions, which cause a minimal increase in the strain energy. When the reduced form of yttrium-doped $BaTiO_3$ was oxidized by annealing in air at 1350 °C, which is above the eutectic temperature in the system $BaTiO_3$–$Ba_6Ti_{17}O_{40}$ (according to the phase diagram the eutectic temperature is 1332 °C), the phase $Ba_6Ti_{17}O_{40}$ partially melted and changed into the Ti-rich compound $Ba_4Ti_{13}O_{30}$, which is stable at that temperature [21]. The reaction is reversible, and during slow cooling from the oxidation temperature the melt reacts with $BaTiO_3$ and Ti-rich phase to form $Ba_6Ti_{17}O_{40}$. After oxidation above the eutectic temperature, the $Ba_6Ti_{17}O_{40}$ precipitates had a globular shape. In this case, the precipitate has a shape with minimal surface, hence the shape of a sphere.

XRPD and electron microscopy showed that the second phase, which precipitated on oxidation of sample with a high yttrium concentration ($Ba_{0.975}Y_{0.025}Ti^{4+}_{0.975}Ti^{3+}_{0.025}O_3$) was the $Y_2Ti_2O_7$ phase. The precipitates of this phase were found in two different shapes. Fig. 4 shows a small precipitate (~0.2 μm in size) in an oxidized sample with nominal composition $Ba_{0.975}Y_{0.025}Ti^{4+}_{0.975}Ti^{3+}_{0.025}O_3$. This precipitate has a cuboid shape. TEM analysis suggested that there is a certain orientational relationship between the precipitate and the perovskite matrix since the outer surfaces of cubic precipitate lie parallel to the {100} plane of perovskite grain.

In addition to rectangular bulk precipitates, the $Y_2Ti_2O_7$ phase also was found in globular shape. Fig. 5 shows a spherical precipitate of ~1 μm size, and SAED shows that it is oriented in the ⟨211⟩ direction. Most probably, the $Y_2Ti_2O_7$ phase start to precipitate forming a nucleus, which forms low-energy interfaces with the perovskite matrix. When the precipitates are small, they retain specific orientation regarding the matrix and have cuboid shape. With increasing precipitates' size, the precipitates tend to minimize surface energy by forming spheres. Those larger precipitates grow independently on the matrix and the orientational relationship with the matrix is lost.

The results obtained show that in the reduced form of yttrium-doped barium titanate the excess yttrium charge is compensated by electrons due to partial change of Ti^{3+} to Ti^{4+}. When the reduced form of yttrium-doped barium titanate ($Ba_{1-x}Y^{\bullet}_{x}Ti^{4+}_{1-x}Ti^{3+}_{x}O_3$) is exposed to oxidizing conditions, the excess charge is compensated by the formation of vacancies in the titanium sublattice with precipitation of Ti-rich phases.

This mechanism of charge compensation is observed in the samples doped with a small amount of yttrium (not more than solubility limit in barium sublattice under oxidation conditions). If the yttrium content is higher than the solubility limit, then in addition to the $Ba_6Ti_{17}O_{40}$ phase the $Y_2Ti_2O_7$ phase precipitates.

Temperature dependences of the resistivity of the materials synthesized in vacuum, and also after oxidation at high temperature in air are shown in Fig. 6. The resistivity of the samples synthesized in reducing atmosphere ($P_{O_2} = 10^{-4}$ Pa) decreases with rising temperature. After oxidation in air at high temperature, regions

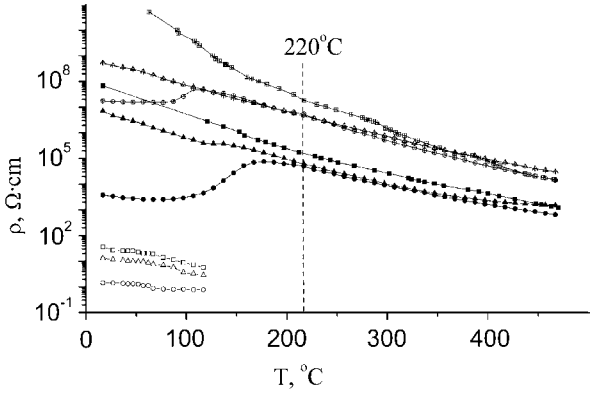

Fig. 6. Temperature dependence of the resistivity of yttrium-doped barium titanate with nominal composition $Ba_{0.99}Y_{0.01}Ti^{4+}_{0.99}Ti^{3+}_{0.01}O_3$ (○, ●, ⊕), $Ba_{0.975}Y_{0.025}Ti^{4+}_{0.975}Ti^{3+}_{0.025}O_3$ (△, ▲, ⧋) and $Ba_{0.96}Y_{0.04}Ti^{4+}_{0.96}Ti^{3+}_{0.04}O_3$ (□, ■, ⊞) after sintering in reducing atmosphere, $P_{O_2} = 10^{-4}$ Pa (○, Δ, □), and after oxidation in air at 1150°C (●, ▲, ■) and 1350 °C (⊕, ⧋, ⊞).

with PTCR appear in the plots of resistivity vs. temperature $\rho(T)$.

According to Heywang model, a potential barrier forms at grain boundaries of the semiconducting ceramics, whose magnitude decreases in the ferroelectric temperature range due to internal fields caused by spontaneous polarization [22]. The potential barrier arises due to acceptor levels at grain boundaries, which are associated with forming by acceptor impurities (for example, 3*d*-metals [23]), oxygen sorption [24,25], and cation vacancies [26,27]. The results of investigations of complex impedance and complex electric module in a wide frequency range allow one to distinguish three areas in doped PTCR barium titanate: semiconducting grain interior, high-resistance grain boundary, and outer grain layer with higher resistance in comparison with grain, which lies between grain and grain boundary [28–31]. This can be represented by an equivalent circuit consisting of three series-connected parallel RC elements [30].

Initially, the results were obtained in the form of complex impedance plots of $Z'(Z'')$, which are convenient for identifying the components of the equivalent circuit. In analyzing experimental data, we also used frequency dependences of Z'' and M'' [28–30,32,33].

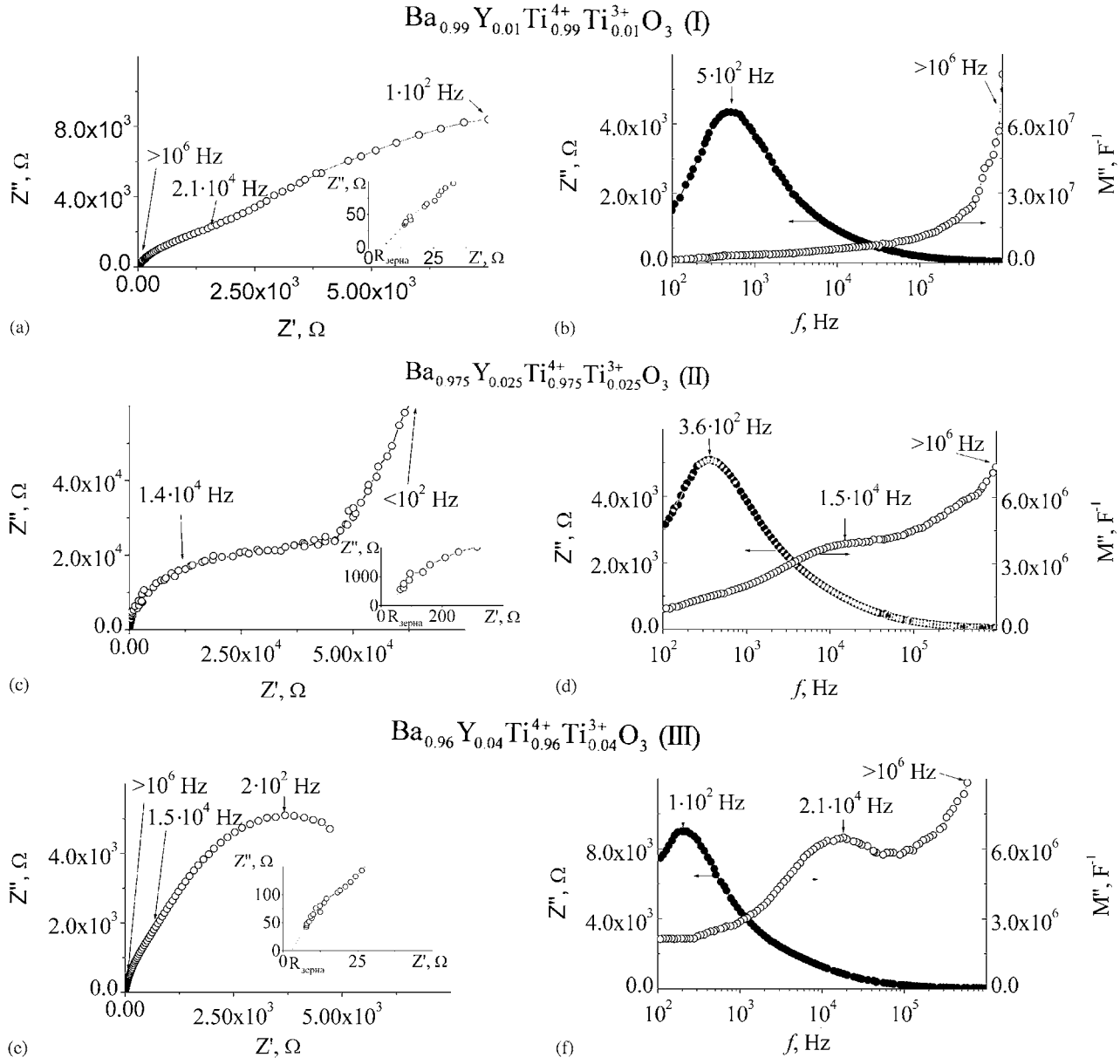

Fig. 7. Nyquist diagrams (a, c, e) and frequency dependences of the imaginary part of impedance Z'' and electric module M'' (b, d, f) of reduced yttrium-doped barium titanate with nominal composition $Ba_{0.99}Y_{0.01}Ti^{4+}_{0.99}Ti^{3+}_{0.01}O_3$ (a, b), $Ba_{0.975}Y_{0.025}Ti^{4+}_{0.975}Ti^{3+}_{0.025}O_3$ (c, d) and $Ba_{0.96}Y_{0.04}Ti^{4+}_{0.96}Ti^{3+}_{0.04}O_3$ (e, f) after oxidation in air at 1150 °C; $T_{invest.} = 220$ °C.

In the present work, the comparative impedance investigations were carried out at a temperature of 220 °C, where there was no influence of PTCR effect, as we can see from the results of measurements of the resistivity of reduced and oxidized samples (see Fig. 6). Figs. 7 and 8 show Nyquist diagrams $Z''(Z')$ and frequency dependences of the imaginary part of impedance Z'' and electric module M'' of the reduced form of yttrium-doped barium titanate with the nominal compositions $Ba_{0.99}Y_{0.01}Ti^{4+}_{0.99}Ti^{3+}_{0.01}O_3$ (I), $Ba_{0.975}Y_{0.025}Ti^{4+}_{0.975}Ti^{3+}_{0.025}O_3$ (II) and $Ba_{0.96}Y_{0.04}Ti^{4+}_{0.96}Ti^{3+}_{0.04}O_3$ (III) after oxidation in air at various temperatures, and Table 1 lists the characteristics of the observed peaks. It should be noted that the real dependences in Nyquist diagrams differ from ideal semicircles. It is possible to take this difference into account using constant phase elements (CPE). CPE is frequently used for diffusion areas and is defined by two parameters, Q and n,

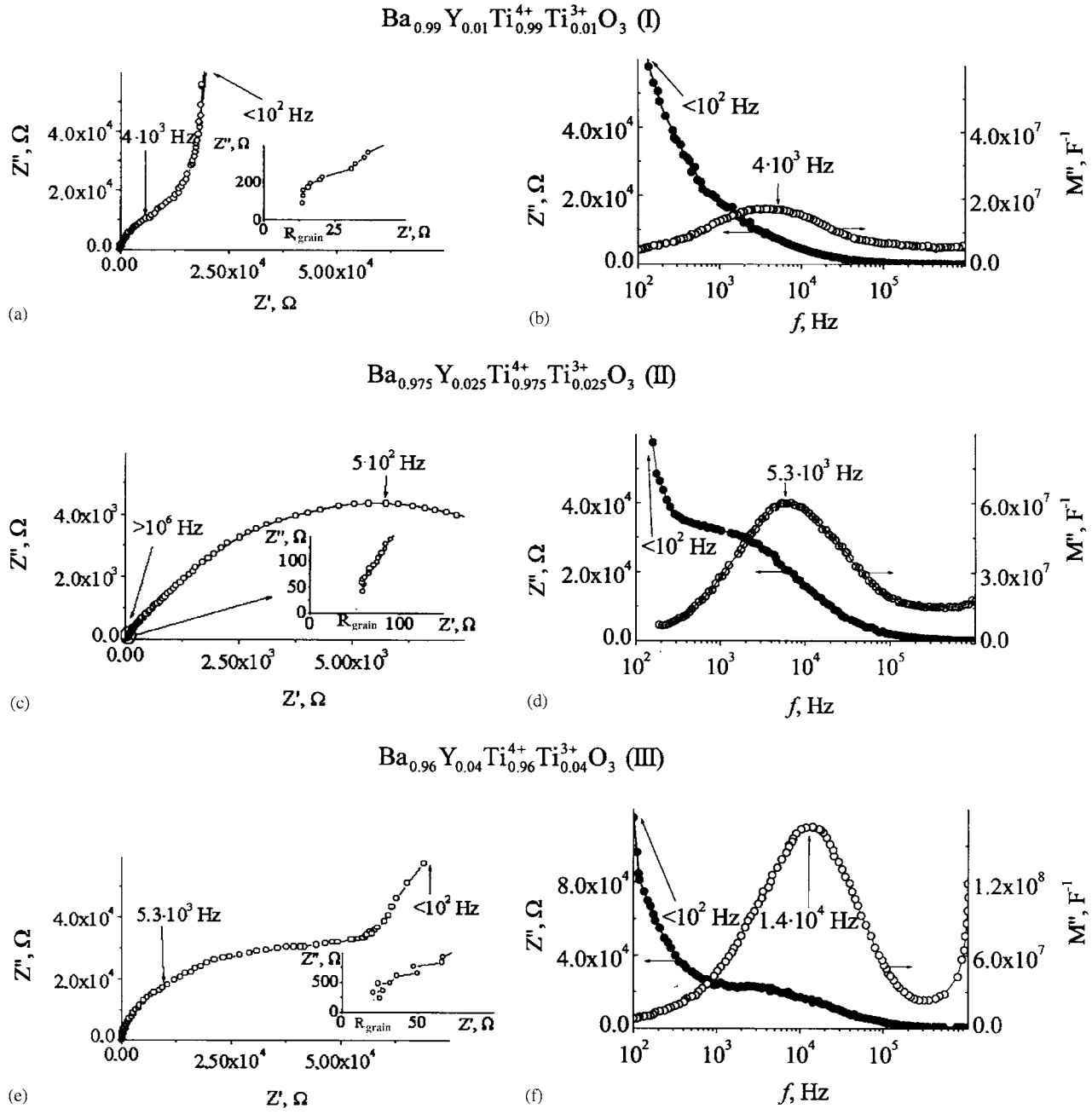

Fig. 8. Nyquist diagrams (a, c, e) and frequency dependences of the imaginary part of impedance Z'' and electric module M'' (b, d, f) of reduced yttrium-doped barium titanate with nominal compositions $Ba_{0.99}Y_{0.01}Ti^{4+}_{0.99}Ti^{3+}_{0.01}O_3$ (a, b), $Ba_{0.975}Y_{0.025}Ti^{4+}_{0.975}Ti^{3+}_{0.025}O_3$ (c, d) and $Ba_{0.96}Y_{0.04}Ti^{4+}_{0.96}Ti^{3+}_{0.04}O_3$ (e, f) after oxidation in air at 1350 °C; $T_{invest.} = 220$ °C.

Table 1
Characteristics of peaks in impedance and electric module plots of ceramics based on barium titanate after oxidation in air at various temperatures

Area of ceramics Peak in plot	Grain boundary $Z''(f)$				Outer grain layer $M''(f)$				Grain $M''(f)$	R_{total}, kΩ
Composition	f^1_{max}, Hz	$R_{boundary}$, kΩ ($R \approx 2Z''_{max}$)	$Q_{boundary}$, nF ($Q \approx 1/\omega_{max}R$)	n	f^2_{max}, Hz	$Q_{outer\ layer}$, nF ($Q \approx 1/2M_{max}$)	$R_{outer\ layer}$, kΩ ($R \approx 1/\omega_{max}Q$)	n	f^3_{max}, Hz	
Oxidation in air at 1150 °C										
$Ba_{0.99}Y_{0.01}Ti^{4+}_{0.99}Ti^{3+}_{0.01}O_3$	500	8.0	30	0.87	—	—	—	—	$>10^6$	8.0
$Ba_{0.975}Y_{0.025}Ti^{4+}_{0.975}Ti^{3+}_{0.025}O_3$	360	8.6	29	0.78	15000	4.6	0.5	0.89	$>10^6$	9.1
$Ba_{0.96}Y_{0.04}Ti^{4+}_{0.96}Ti^{3+}_{0.04}O_3$	100	10.1	27	0.77	21000	2.8	1.1	0.89	$>10^6$	11.2
Oxidation in air at 1350 °C										
$Ba_{0.99}Y_{0.01}Ti^{4+}_{0.99}Ti^{3+}_{0.01}O_3$	$<10^2$	630	5.2	0.94	3800	2.8	11	0.90	$>10^6$	830
$Ba_{0.975}Y_{0.025}Ti^{4+}_{0.975}Ti^{3+}_{0.025}O_3$	$<10^2$	890	4.8	0.92	5300	0.5	53	0.87	$>10^6$	970
$Ba_{0.96}Y_{0.04}Ti^{4+}_{0.96}Ti^{3+}_{0.04}O_3$	$<10^2$	1700	4.6	0.90	14000	0.1	85	0.77	$>10^6$	2270

according to formula $Z = Z_0/(j\omega)^n$. If $n = 1$, then CPE is equivalent to a capacitor with capacity Q. If $n<1$, this indicates a frequency dependence of capacity, i.e. dispersion [34].

The grain core has a relatively small resistance and capacity; therefore, its peak is observed at high frequencies ($>10^6$ Hz), and the dependence $Z''(Z')$ can be used for the graphic determination of grain resistance (Fig. 7a). In plots of $Z''(f)$ for compositions (I), (II), (III) after oxidation in air at 1150 °C only one peak is observed at 5×10^2, 4×10^2, 1×10^2 Hz, respectively (Fig. 7b,d,f), which describes the variation of electrophysical properties of dielectric grain boundaries with yttrium concentration. In the plot $M''(f)$ for compositions (I)–(III) a significant increase in M'' with f is observed, indicating that there is maximum $M''(f)$ at frequencies $>10^6$ Hz, which describes the electrophysical properties of semiconducting grain (Fig. 7b). At the same time, for compositions (II) and (III) there are additional peaks in plots of $M''(f)$ at frequencies of 1.5×10^4 and 2.1×10^4 Hz, respectively, which relate to change of electrophysical properties of the outer grain layer (Fig. 7d and f).

Similar regularities are observed for dependences of Z'' and M'' for samples after oxidation in air at 1350 °C (Fig. 8). In this case, the resistance of the grain boundaries becomes higher, which manifests itself by a shift of $Z''(f)$ peak towards low frequencies (see Fig. 8); the properties of the outer layer also change: its resistance increases and the capacity decreases (see Table 1).

The above data show that on oxidation in air the resistance of the outer grain layer of doped barium titanate considerably increases with yttrium concentration (compositions (II) and (III)) in comparison with composition (I), which has minimum yttrium concentration. The increase in the resistance of the outer grain layer may be accounted for both by the formation of the phases $Ba_6Ti_{17}O_{40}$ and $Y_2Ti_2O_7$, whose existence is confirmed by XRPD analysis and microscopic investigation, and by additional acceptor levels formed by cation vacancies in $Ba_{1-x}Y_xTi^{4+}_{1-x/4}(V''''_{Ti})_{x/4}O_3$ phase on oxidation.

4. Conclusions

The investigations carried out showed the following:

Barium titanate doped with low yttrium concentration oxidizes with precipitation of the $Ba_6Ti_{17}O_{40}$ phase, which has a well-defined orientational relationship with the perovskite matrix. The form of particles precipitated depends on the temperature of oxidation and on the mode of nucleation. After oxidation at 1150 °C, the $Ba_6Ti_{17}O_{40}$ phase was found in two different forms: in the form of bulk precipitates, when they heterogeneously nucleated and in the form of plates, when they

homogeneously nucleated, and after oxidation at 1350 °C particles were found in a globular form.

Barium titanate doped with high yttrium concentration oxidizes with precipitation of the $Ba_6Ti_{17}O_{40}$ and $Y_2Ti_2O_7$ phases. In this case, the phases also have a well-defined orientational relationship with the perovskite matrix. The particles of the $Y_2Ti_2O_7$ phase also precipitate in two different forms: as rectangular bulk precipitates and as a globular precipitates.

Oxidation of the reduced form of doped barium titanate results in an increase in the resistance of the outer grain layer, which lies between grain boundary and grain. The resistance of the outer layer increases with the concentration of donor dopant (yttrium) and oxidation temperature due to the formation of the phases $Ba_6Ti_{17}O_{40}$ and $Y_2Ti_2O_7$ and to the appearance of additional acceptor levels due to cation vacancies in $Ba_{1-x}Y_xTi^{4+}_{1-x/4}(V''''_{Ti})_{x/4}O_3$ phase on oxidation.

References

[1] O. Saburi, J. Phys. Soc. Japan 14 (1959) 1159–1174.
[2] V.J. Tennery, R.L. Cook, J. Am. Ceram. Soc. 44 (1961) 187–193.
[3] B.A. Rotenberg, Yu.L. Danilyuk, Izv. AN SSSR. Ser. Fiz. 31 (1967) 1824–1827.
[4] A.G. Belous, O.I. V'yunov, B.S. Khomenko, Inorg. Mater. 34 (1998) 725–729.
[5] O. Okazaki, Semiconducting Barium Titanate, Gakkensya, 1977.
[6] F. Kreger, Chemistry of Imperfect Crystals, Moscow, 1969.
[7] D. Makovec, Z. Samardzija, M. Drofenik, J. Am. Ceram. Soc. 87 (7) (2004) 1324–1329.
[8] D. Makovec, M. Drofenik, J. Am. Ceram. Soc. 83 (2000) 2593–2599.
[9] M.T.Buskaglia, V.Buskaglia, M.Viviani, P.Nanni, Ninth International Conference on Modern Materials & Technologies, Florence, 1998.
[10] G.P. Kostikova, Yu.P. Kostikov, Chemical Processes During Doping of Oxides, Petersburg, 1997.
[11] J. Zhi, A. Chen. Y. Zhi, P.M. Vilarihno, J.L. Baptista, J. Am. Ceram. Soc. 82 (1999) 1345–1348.
[12] A.G. Belous, V.V. Dem'yanov, M.F. Dubovik, Izv. AN SSSR, ser. Neorg. Mat. 14 (6) (1978) 1132–1137.
[13] H.T. Evans, Acta Crystallogr. 14 (1961) 1019–1026.
[14] M. Kato, T. Kubo, J. Chem. Soc. Japan 70 (1967) 840–843.
[15] T. Negas, R.S. Roth, H.S. Parker, D. Minor, J. Solid State Chem. 9 (1981) 287–307.
[16] M.E. Lines, A.M. Glass, Principles and Applications of Ferroelectrics and Related Materials, Oxford, 2001.
[17] K. Okazaki, Technology of Ceramic Dielectrics, Moscow, 1976.
[18] J.-I. Itoh, D.-C. Park, N. Ohashi, J. Appl. Phys. Japan 41 (2002) 3798–3803.
[19] V. Krasevec, M. Drofenik, D. Kolar, J. Am. Ceram. Soc. 70 (1987) 93.
[20] D. Makovec, D. Kolar, J. Am. Ceram. Soc. 80 (1997) 45–52.
[21] T. Negas, R.S. Roth, H.S. Parker, D. Minor, J. Solid State Chem. 9 (1981) 287–307.
[22] W. Heywang, Solid State Electron. 3 (1961) 51–58.
[23] H. Ueoka, Ferroelectrics 7 (1974) 351.
[24] G.H. Jonker, Halogen, Mater. Res. Bull. 2 (1967) 401–407.
[25] H. Igarashi, S. Hayakawa, K. Okazaki, Jpn. J. Appl. Phys. 20 (1981) 135.
[26] J. Daniels, K.H. Hardtl, R. Wernicke, Philips Tech. Rev. 38 (1978) 73–82.
[27] G.V. Levis, C.R.A. Catlow, J. Phys. Chem. Solids 47 (1986) 89–97.
[28] D.C. Sinclair, F.D. Morrison, A.R. West, Int. Ceram. 2 (2000) 33–37.
[29] F.D. Morrison, D.C. Sinclair, A.R. West, J. Am. Ceram. Soc. 84 (2001) 474–476.
[30] F.D. Morrison, D.C. Sinclair, A.R. West, J. Am. Ceram. Soc. 84 (2001) 531–538.
[31] D. Makovec, N. Ule, M. Drofenik, J. Am. Ceram. Soc. 84 (2001) 1273–1280.
[32] G.H. Jonker, Solid-State Electron. 7 (1964) 895–903.
[33] P.K. Dutta, M.A. Alim, J. Appl. Phys. 35 (1996) 6145–6152.
[34] J.R. Macdonald, Impedance Spectroscopy, New York, 1987.